The application of different typological and structural MOFs-based materials for the dyes adsorption

Danni Jiang [a,b,1] Ming Chen[a,b,1] Han Wang [a,b,1] Guangming Zeng [a,b,*]

Danlian Huang [a,b,*] Yang Liu[a,b] Wenjing Xue [a,b] ZiWei Wang[a,b]

a College of Environmental Science and Engineering, Hunan University, Changsha, 410082, PR China,

b Key Laboratory of Environmental Biology and Pollution Control, Hunan University, Ministry of Education, Changsha 410082, PR China.

[1] These authors contribute equally to this article.

Abstract

Dye wastewater is an universial problem that restricts sustainable development. Adsorption is an effective technique for water purification due to high efficiency, economic feasibility and operational ease. Metal-organic frameworks (MOFs) as adsorbent has attracted great attention on account of exceptionally high porosity, compositional and structural diversity, and highly tunable pore shape/size and surface functionality. This review focused on recent progress in reported different typological and structural MOFs as superior adsorbents for the efficient removal of toxic dyes. Optimized, Modified, defective, compositive and derived MOFs could improve the adsorption performance of MOFs. In particular, some MOFs-based adsorbent with special structure was concerned. Aspects related to the interaction mechanisms between dyes and MOFs-based materials are systematically summarized, including adsorption performance, kinetics and thermodynamics and mechanism. Finally, we propose our personal insights in the hope of MOFs-based material better used for environmental pollution management.

Key words: Metal-organic framework; dyes; adsorption; multidimensional; mechanism

Content

1. Introduction

Dyes from a variety of chemical industries have been considered to the main component of sewage. Textile industries consume over 700 000 tons of dyes which are the one of top three pollutants, however, many reactive dyes are toxic, and have a risk of teratogenic and carcinogenic mutations [1-4]. Among the many processing technologies, adsorption is considered to green and environmentally friendly one due to high efficiency, easy opration and economic feasibility [5-8].

Metal–organic frameworks (MOFs), as a new star of porous material, occupied an important position in the field of adsoeption and separation take the advantage of high specific surface area and porosity, tunable structure and function. Recently, there have been many reviews on the synthesis and application of MOFs [9-20]. Some reviews focused on the synthesis of mesoporous MOFs and potential applications [9,10], while others concerned the removal performance of different pollutants by MOFs, such as heavy metal pollutants [11-13], toxic and radioactive metal ions [14], aromatic pollutants [15,16] and azo dye [17]. Other reviews focused on adsorption mechanisms [18-20].

This review focused on recent advances in reported different typological and structural MOFs as superior dye adsorbents. Optimized, modified, defective, compositive and derived MOFs could improve the adsorption performance of MOFs. Fig. 1. showed the whole content of the manuscript. (i) Optimized MOFs with special structure, including one-dimensional (1D) chains, two-dimensional (2D) layers, and three-dimensional (3D) supraframework have received attention; (ii) mixed-metal and linker-functionalization are the main forms of the modified MOFs; (iii) MOFs designed with defects contributed to the formation of defective active sites; (iv) MOFs-based composites originating from the combination of MOFs with other functional materials, designed to improve surface area, adsorption capacity and easy of separation; (v) derived MOFs refer to the direct carbonization of MOFs as raw materials. The MOF-derived nanostructures acted as adsorbent depended on unique advantages:1) designability of chemical composition by various MOFs; 2) expanded

specific surface area and porosity; 3) low cost and easy synthesis. In addition, aspects related to the interaction mechanisms between dyes and MOFs-based materials are systematically summarized, including adsorption performance, kinetics and thermodynamics and mechanism. Finally, we propose our personal insights in the hope of MOF-based material better used for environmental pollution management.

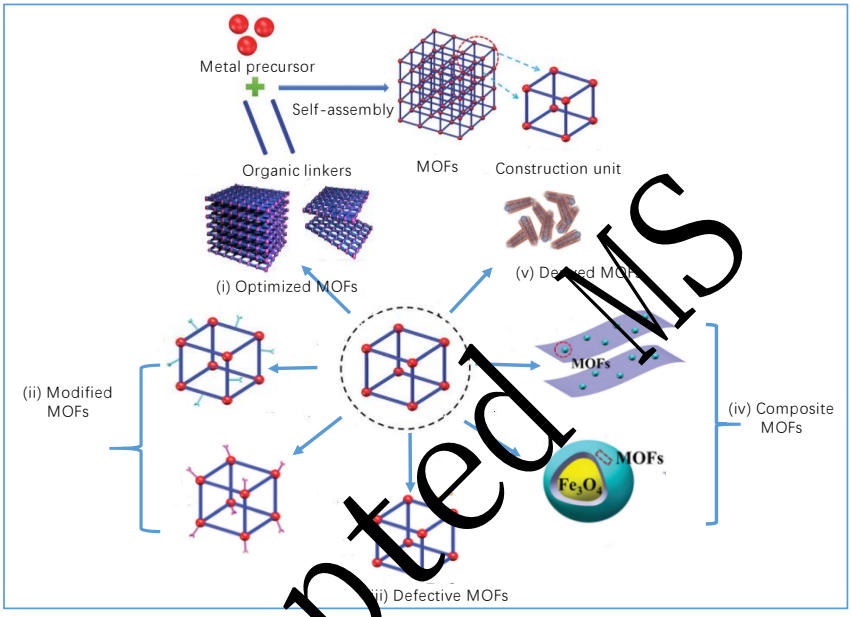

Fig. 1 Graphical representation of MOFs and strategies for boosting the adsorption performance of MOFs-based adsorbent. (reprinted with permission from ref.20. Copyright (2018).The Royal Society of Chemistry).

2. Optimized MOFs as dye adsorbents

Dyes are difficult to remove and to degrade from water. However, MOFs as adsorbent show strong performance by exceptionally high porosity, compositional and structural diversity, and highly tunable pore shape/size as well as surface functionality [21-23]. Among them, Fe-based MOFs as adsorbent by providing potential unsaturated metal sites for strong adsorption interaction have received wide attention [24-28]. For example, MOF-235 (Fe-based MOF) can efficiently adsorb both cationic and anionic dyes, the adsorption effect of which is superior to activated carbon [24]. MOF-235 is effective not only for methyl orange (MO) but also for methyl red (MR)

[25]. Similarly, MIL-100 (Fe, Cr) could adsorb Methyl Blue (MB) with the maximal adsorption capacity of 211.8 and 1045.2 mg/g, suggesting that the degree of difference observed between the adsorption performance of MIL-100 (Fe) and MIL-100 (Cr) [26]. MIL-100 (Fe) was also an decolorizer for malachite green (MG) [27]. Notably, in the synthesis process, the use of hazardous reagents limited mass production of MOFs, however, NMIL-100 (Fe) with hydrpfluoric acids (HF)-free by environmental-bengin synthetic strategy was prepared and was applied as an highly effective adsorbent [28]. Other common transition metals used for the building of MOFs-based adsorbent included Cu, Mn, Cd, Zn and Al et al. Mesoporous Cu-BTC was effective for MB (200 mg/g) [29] and mesoporous Mn-BTB based on the a tritopic linker 1,3,5-tris(4-carboxyphenyl)benzene (H_3BTB) was applied to the decolorization of MB [30]. Both TMU-7 (Cd (II)-based MOF) (79 mg/g) and TMU-39 (Zn (II)-based MOF) (53 mg/g) have similar adsorption effect of Congo red (CR) [31, 32]. Cd (II)-based MOF ($[Cd(INA)_2(H_2O)]$) JSB could adsorb MO with the maximum adsorption capacity 166 mg/g [33]. Fumaric acid (FA) and succinic acid (SA) were chosen as ligands to construct Al-based MOFs (Al-FA and Al-SA), which exhibited superior affinities toward mono- and di-azo dyes with maximun adsorption capacities of 559.28 and 332.48 mg/g, respectively [34].

Limited adsorption capacity and water instability make the adsorption performance plain, however, some special structural MOFs, especially multidimensional MOFs such as zero-dimensional (0D) clusters [35, 36], 1D chains [37] and 2D layers [38-40] and 3D pillar [41-44] with high specific surface area, porosity and channels matching organic pollutants exhibited high adsorption performance. 2D graphene-like BUC-17 ($[Co_3(tib)_2(H_2O)_{12}](SO_4)_3$) exhibited the good decolorization effect towards CR and the maximum adsorption capacity of which was 4923.7 mg/g. Structurally, the octahedral geometry of the Co(II) atom in BUC-17 is completed by two nitrogen atoms from two different tib ligands and four oxygen atoms from coordinated water molecules, which lie in the four sites of the equatorial plane. Six Co (II) atoms are connected by six tib ligands to form a graphene-like hexagonal pore subunit with an

aperture size of *ca.* 2.36 nm. The absorption kinetics and absorption thermodynamics fitted the pseudo-second-order and the Langmuir model, respectively. Similar to the adsorption of CR onto AC, the adsorption process was endothermic confirmed by the the positive values of ΔH_0 (92.62 kJ mol^{-1}). The positive surface charge, π–π stacking interactions, ion-exchange, and hydrogen-bonding along with the effect of mesopores could be responsible for the fast adsorption [45]. A novel 1D discrete single-walled metal-organic nanotube (JLUI-MONT1) with a rare armchair (3,3) carbon nanotube topology is an excellent adsorbent for basic red 9 (BR9) and basic violet 14 (BV14). There are two possible reasons for the amazing adsorption capacity: (1) the framework has sufficient space to accommodate the dyes; (2) the channels of JLU-MONT1 well swallowed the triangle-shaped molecules [46]. 2D MOFs frenqutly based on the building unit of multitopic carboxylic ligands, whereas metal-organic polyhedral cage-like assemblies based on angularly bent ligands is a common strategy. Based on the isophthalic acid (H_2IP) and its 5-substituted derivatives carboxylic ligands, they connected to typical Cu2 paddle-wheels in infinite 2D sheets in the (001) plane to bulid 2D Cu-based MOF, which exhibited adsorption rates in the order MB>RhB (Rhodamine B) >MO [46]. The other adsorbents are effective for MB and MO including 2D Ni(II)-based MOF $[Ni_4(D\text{-}cam)_2(D\text{-}Hcam)_4(bpzpip)_4(H_2O)_2]$ [47], 2D Zn(II)-based MOF $\{[Zn_2(HBTC)_2(L)(H_2O)_2](C_2H_5OH)_3\}_n$ [48] and $\{[Zn_2(L)(H_2O)(DMA)]\cdot DMA\cdot H_2O\}_n$ [49]. Interconnection of $[Ni_2(m\text{-}H_2O)(O_2C)_4N_4]$ as secondary building units (SBUs) through bpzpip ligands as single-edged generates a 2D undulated nickel-bpzpip (4,4)-sheet structure. Then, the 2D achiral nickle-bpzpip sheets intersected by the 1D chiral nickel-camphorate chains to result in a 2D uninodal six-connected sheet featuring the 3^6-hxl topology which are beneficial for MB adsorption with the saturated adsorption amount of 185.5 mg/g [47]. $\{[Zn_2(HBTC)_2(L)(H_2O)_2](C_2H_5OH)_3\}_n$ in view of mixed ligands strategy is a 2D network composed of a $[Zn_2(HBTC)_2(H_2O)_2]_n$ motif linked via terminal nitrogen atoms of L (L = 1,4-bis(4-pyridyl)-2,3-diaza-1,3-butadiene), which can effectively adsorb RhB, MB, and MV (Methyl violet) (24.36, 21.55 and 17.15 mg/g) [48]. The

spacer $L(NH_2)_2$ has a flattened topology that can engage in multiple strong directional interactions in a single plane favors the formation of layer structures. Similarly, considering the mixed ligands strategy, $\{[Cd(ipa)(L(NH_2)_2)(DMF)]\ H_2O\}_n$ auquired a 2D square net structural arrangement and exhibited selective adsorption towards crystal violet (CV) dye. Weak forces including π-π interactions as well as hydrogen bonding and interactions with free basic amine sites are responsible for the adsorption process [50].

MOF nanosheets, as a new important member of 2D materail family, is an candiadate for adsorption materials because of their nanometer-sized thickness along with the arrangement of regular pore. MOFs nanosheets provide convenient conditions for capture of adsorbents [51-54]. $[Zn_2(Benzimidazole)_3(OH)(H_2O)]_n$ nanosheets was prepared from layered $Zn_3(Bim)_3$ precursors via a modified top-down method [55]. The $Zn_2(Bim)_3$ nanosheets-based molecular sieve membranes derived from bulky particles exfoliation revealed an exceptional gas separation performance [56]. A bottom-up synthesis strategy was applied to prepare highly crystalline MOF nanosheets with superior adsorption properties [57]. Although the current research of MOF nanosheets focused on gas adsorption, it will be important to apply them to dye adsorption.

3D pillared-layer MOFs (PL-MOFs) are types of MOFs that are constructed from many parallel pillar and 2D layers [58]. Among these, the most important characteristic of flexible pillars is that it can shrink and expand in response to guest molecules [59]. Common strategy including both dual-ligand and mixed-ligand used to construct PL-MOFs. Among them, two kinds of classis PL-MOFs are well-konwn. The first one is that poly-carboxylate ligands link $[M_2(COO)_4]$ paddlewheel SBUs to generate layer structure, along with bridge adjacent layers build by N-contained ligands such as bupyridine or pyrazine to form the final framework. Another one is the SIFSIX series, in which N-contained ligands coordinate with single metal centres to form layers [60]. A new Zn-based MOF $(Zn_4(D\text{-}cam)_3(OHbim)_2$ based on cationic $[Zn_2(COO)_3]^+$ SBUs. Interestingly, each $[Zn_2(COO)_3]^+$ SBU cooridinate with three

D-cam ligands to form a cationic layer, which is pillered by -a charged OH-bim ligands to form the neutral framework with rare sqp topology [61]. 3D tbo network FJ1-H-U1 (Ur-based MOF) exhibited the selective dye adsorption by considering that the planar triangular $[UO_2(COO)_3]^-$ units could be simplified to the 3-connected node. Tetrakis (4-carboxyphenyl)ethylene (H_4TCPE) was chosen as the organic ligand because of the freely rotated C-C bonds resulted in a nonplanar conformation [62]. Based on a classical $[Cu_2(COO)_4]$ paddlewheela, hexa-nuclear $[Cu_6O_2(SO_4)_6]$ cluster, and a 3-conncted hetero-N, O donoe ligand, anionic framework JLU-Liu39 was build and showed good adsorptive performance towards cationic dyes (308mg/g). The whole 3D framework possesses a (3,4,4)-connected fjh topology and facilitating conditions for dye enrichment such as a large window size of 25.3Å with approximately 75.8% of the cell volume [63]. By inspired, JLU-Liu18 displays a rare occurrence of 9-connected, trinuclear $[In_3O(COO)_6N_3]$ SBUs in a porous crystal, with high adsorption [64]. 3D pillar layer structure of $[Co(biimb)(BPDC)(H_2O)_2]\cdot DMA\cdot 10H_2O$ (1) based on tripodal imidazole-containing ligand biimb and linear dicarboxylic acid H_2BPDC can selectively adsorb MO (20 mg/g) due to the size matching effect. Two imidazole groups of biimb connect Co2 to form (4,4) grid 2D layer and the coordination between the third imidazole group and Co1 acts as pillars to finish the 3D pillar-layered framework [65]. Another 3D stable Cu-based MOF $[Cu_4(1,4\text{-ndc})_4(L)_2]H_2O\cdot 2DMF$ exhibited high adsorption performane for RhB attributed to 6-connected two-fold interpenetrating pcu framework constructed from binuclear Cu(II) clusters and coexist hydrogen-bonding acceptors and donors [66]. Five isostructural pillared-layer MOFs (Zn-based MOFs) have been constructed with different interlayer distances, pore volumes and pore surface functionalizations controlled by size-alterable pillar ligands as well as selection of layers, which exhibited differential adsorption performance [67]. Other 3D MOFs included Co-based MOF ($\{[Co(oba)(bpe)](H_2O)_{0.25}\}_n$) ($H_2$oba=4,4'-oxy(bis)benzoic acid, bpe=1,2-bis(4-pyridyl)ethene) and $[Zn(\mu_4\text{-ppda})(\mu\text{-abpy})0.5]_n$ (ppda=1,4-phenylenediacetate, abpy=4,4'-zaobis(pyridine)) and 3D Zn-based MOF et

al [68-70]. Although MOFs offer sizable and chemically functionalizable three-dimensional porosity, which is facilitate for adsorption applications, their performance was still subjected to unsatisfactory strucrutal and hydrolotic stability along with high surface areas [71].

Structural transformation from one crystalline phase to another without change of content of the unit cell is common, which was realized by varying synthesis condition including ligand, solvent, pH, and temperature [72]. A new hieratchical MOF consisting of Cu(II) centers connected by benzene-tricarboxylates (BTC) is prepared, then, a thermo-induced transformation of a ribbon-like 1D building unit into 2D layers and finally a 3D network was revealed, and specially, the new 3D network have outstanding performance of molecular separation [73]. pH exerted an influence on the phased transformation from the 1D chain $[Mg(Pdc)(H_2O)_3]_n$ to 3D framework $[Mg(Pdc)(H_2O)]_n$ (Pdc=pyridine-2,3-dicarboxylate), and 3D showed higher activity than 1 chain [74]. Based on th different ligands and solvent, three coodination compounds among 0D $Co(tib)(ADC)_2$ (BUC-60), 1D $Zn_3(tib)_2Cl_6$ (BUC-61) and 3D $[Cu_2(tib)_2(MoO_4)Cl]Cl$ (BUC-62) showed different CR adsorption capacity [75]. However, the existing studies couldn't meet the requirements of dye adsorption, more work is needed on multi-dimensional MOFs for dye adsorption.

3. Modified MOFs as dye adsorbents

3.1 On the basis of metal node functionalization

Recently, the strategy of mixed-metal MOFs, in which multiple functionalities are introduced into a single MOF net work, has attracted much scientific interest [76]. It could be considered to be "molecular substituional alloys", where the properties of the modified MOFs could be different from the single constituent phases. The structural flexibility of V-doped MIL-53 is distinct from that of the pure Fe material [77]. The iron doped ZIF-8 (Fe-ZIF-8) was effective for the adsorption of Remazol Deep Black (RDB) [78]. The ZIF-8 doped by iron resulted in lowed pore volume, pore diameter and decreased specific surface area due to partical pore blocage. The electrostatic interaction, the hydrophobic and π-π interactions as well as the

coordination bonds were also responsible for the higher adsorption capacity. Different from the Fe-ZIF-8, ZIF-67 doped by Cu offered increased surface areas [79]. Cobalt (Co) and nickel (Ni) located at iron groups are also used as doping elements. A mixed metal nano-sized crystals CoZn-ZIF-8 was prepared using microwave irradiation with reduced the amount of ligand and solvent which is different from the convential solvotherm method. Similarity of valence states of Co ions in both pure Co-ZIF-8 and the mixed metal was confirmed by the Xray absorption near edge strcuture (XANES). Interestingly, as the Co/Zn ratio in mixed metal ZIFs increases, the metal to nitrogen (M-N) strenching frequencies on IR were observed to be blue-shifed systematically [80]. The blue shift was existed in CoZn-ZIF-8 which was attributed to the fact that the Co-N bond is mechanically more rigid than the Zn-N bond, leading to the smaller effective aperture in CoZn-ZIF-8. Differently, in CdZn-ZIF-8, it was the red shift that can be caused by the less rigid Cd-N than the Zn-N bond [81]. The increased adsorption performance of Co-MOF was found, because Co exsited as metal node which was confirmed by the fact that there is such a promouced effect of the presence of Co on the temperature of the linker decomposition. Co was actually incorparated into the framework and greatly affected the adsorption process. The Co coordination changes depending on the solvent molecules inside the cavities are completely reversible [82]. In addition, Ni and Co are more favorably incorporated in the final mixed-metal MOF-47 (MM-MOF-47) framework with reduced surface area than Mg, and the adsorption can be turned by the incorporation of low-affinity metal sites into the MOF-47 framework [83,84]. Further, the enhanced water stability of modified Ni/Co-MOF-47 provided the possibility for application in dye wastewater.

HKUST-1 was often selected as another modified precursor. Ni/Cu mixed-metal porous material, specifically, Cu (II) cations are partly substituted by Ni (II) enhanced the adsorption property toward CR because of the synergitic effect. The CR adsorption process fitted to the Langmuir model, suggesting that the adsorption sites are mainly monolayer [85]. NiCu-BTC is effective not only for CR but also for methylene MB. In NiCu-BTC, the (100) plane can be considered as the largest

exposed facet, and it changed to (002), (022) and (222) exposed facet after Cu incorpotation, which is thought to be related with the changed adsorption capacity. The common groud between the two is that compared to Cu-BTC, Ni/Cu-BTC offered decreased surface area and total pore volume [86].

Owing to the chemical similarity between Zr^{4+} and Ti^{4+}, the incorporation of Ti^{4+} in UiO-66 may used as adsorbtents for the enrichment of dye. Different from the parent UiO-66, the intensity of the diffraction peaks of the UiO-66 doped by Ti decreased slightly, indicating larger Zr^{4+} in the [Zr-O] clusters replaced by small Ti^{4+} resulted in crystal lattice and suppression of crystal growth for the Ti-UiO-66 MOFs. The Langmuir isotherm model represented to monolayer adsorption and pseudosecond-order model represented to chemical adsorption were found to be suitable to decribe the adorption process [87]. Ce (III) different from Ti (VI) could dope into UiO-66 which increases the number of adsorption sites and promotes π–π interactions between the adsorbate and the adsorbent [88]. However, most researches on the metal node functionalization focused on gas adsorption, the effect on dye adsorption capacity needs to be discussed in future.

3.2 On the basis of linker functionalization

Except the metal node functionalization, the linker functionlization is an effective strategy to turn the physical and chemical properties of MOFs. A primary amine group ($-NH_2$) can be directly introduced into various MOFs since weak metal-amino group bonds could not destroy metal-carboxylic acid bonds [89]. There are different synthetic approaches by which amine fucntionalities can be incorporated into MOFs: (i) postsynthetically ‘grapfting’ amines onto vacant metal coordination sites, (ii) using ligands thay have pendant amines covalently attached and (iii) using ligands in which the amines are embedded within the main backbone of the bridging ligands. Diverse MOFs functionalized by amino group including MIL-125-NH_2, MIL-101-NH_2 and UiO-66-NH_2 et al have been reported. The maximum adsorption capacity of MB was found to be 321.39 mg/g and 405.61 mg/g by MIL-125 and NH_2-MIL-125. The uncoordianted NH_2 group occupied the space of the mesoporous, which was

confirmed by the similar XRD (X-ray diffraction) patterns. Due to the amino-functioanlization, the specific surface area for NH_2-MIL-125 is higher (1028 m^2/g) than that for MIL-125 (470 m^2/g) [90]. The high adsorption capacity was due to the more negative zeta potential (-32.4 mV) of the NH_2-MIL-125 because of the lone pair eletrons in the nitrogen atom and the adsorption process was controlled by pseudo-second-order kinetic equations. NH_2-MIL-125 applied the similar adsorption for three component dye system, including Basic Red 46 (BR46) (1296 mg/g), Basic Blue 41 (BB41) (1257 mg/g), and MB (862 mg/g) [91]. In addition, UiO-66-NH_2 with the more negative zeta potential for the protonation of -NH_2 contributed to higher adsorption capacity for cationic [92]. On the other hand, the decreased surface area was not the decider in the adsorption process. UiO-66-NH_2 is also effective towards four hydrophilic dyes. Different from the increased surface area, this loss of BET surface area and pore size distribution can be ascribed the blocked cages by peripheral amino functional group. Fig. 2 summarized the changes of specific surface area of several functional MOFs. However, the increased BET surface area was not related with the increased adsorption capacity, and they are 633.4 mg/g for Acid blue 92 (AB 92) and 500.2 mg/g for Direct red 80 (DR 80) [93]. The kinetic pseudo-second order model and the thermodynamic Langmuir isotherm model of NH_2-ZIF-8 were consistent with that of ZIF-8. In addition, enhanced dye adsorption capacity by modified MOFs were confirmed in the study of Haque et al., [94], Bibi et al., [95] and Oveisi et al [96].

MOFs with other functional groups modified ligand were also favorable for adsorption. UiO-66s with acidic sites, such as carboxylic and sulfonic acids, have been synthesized for adsorption. The favorable contribution of free -COOH to adsorption could be explained by H-bonding [97]. Another MOF with -COOH demonstrated strong interaction with MB [98]. The surface charge of MOFs altered by the linker functionalization is an interesting finding. The surface charge of the MIL-101 (Cr) was changed inversely derived from the -SO_3H group, thus both MIL-101 (Cr) and MIL-101 (Cr)-SO_3H exhibited different adsorption performance on

ionic dye and cationic dye [99]. Similar result was also found in the work of Luo et al, MIL-101 (Cr)-SO_3H was benefit for the enrichment of cationic dyes, including MB and MG [100]. Thus, modified ligand could improve the water stability of MOFs. Meanwhile, ligand functionalization affected the specific surface area as well as the surface charge, comparing to the specific surface area, the surface charge played more important role in selective adsorption of dyes, which was consistent with the main mechanism of electrostatic attraction.

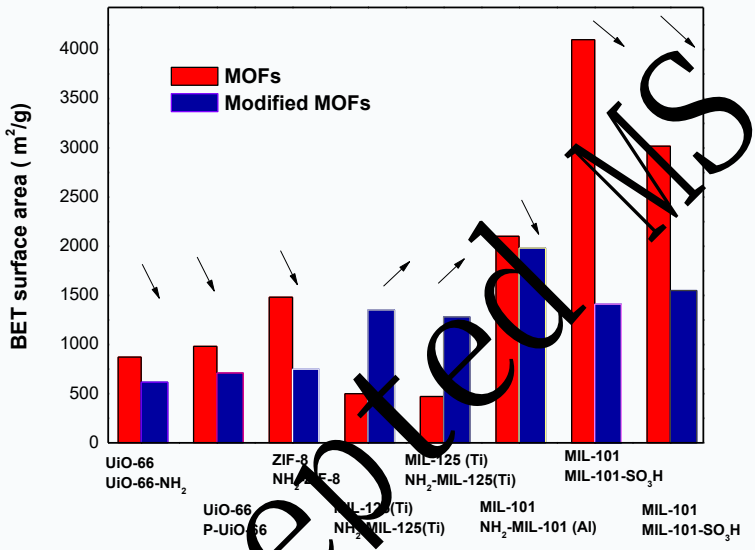

Fig. 2 The changed BET surface area of the MOFs on the basis of linker functionalization

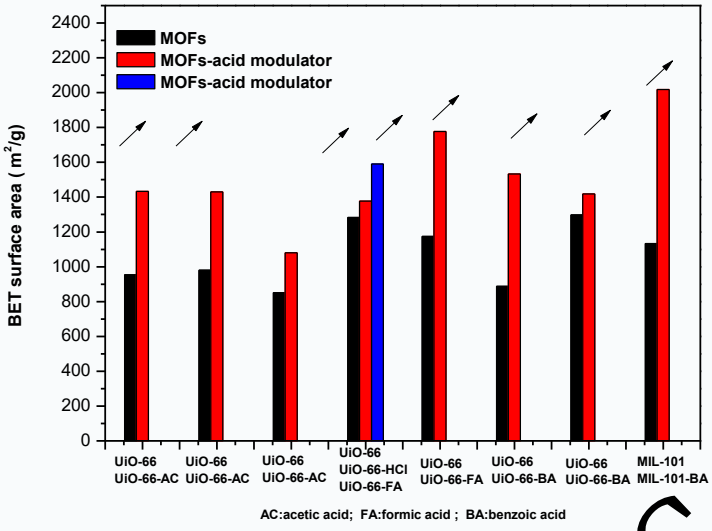

Fig.3 The changed BET surface area of the MOFs on the basis of modulator

Table 1. Recent progress in optimized, modified and defective MOFs as dye adsorbent

Optimized MOFs as dye adsorbent

MOFs	Ligand	S_{BET} (m^2/g)	Q_0	Adsorption kinetics	Adsorption thermodynamics	Mechanism	Reference
MOF-235	H_2BDC		MO 477	Pseudo second-order kinetic model	Langmuir isotherm	Electrostatic interaction, π-π interaction	[24]
MIL-53	H_2BDC	23	MR 183.5	Pseudo second-order kinetic model	Langmuir isotherm	Electrostatic interaction, π-π interaction, the breathing effect	[25]
MIL-100 (Fe)	H_3BTC		MB 1045.2	Pseudo second-order kinetic model	Langmuir isotherm	Electrostatic interaction	[26]
MIL-100 (Cr)			MB 211.8				
MIL-100(Fe)	H_3BTC	1626	MG 146	Pseudo second-order kinetic model	Langmuir isotherm	Electrostatic interaction, π-π interaction, Lewis acid-base interaction	[27]
NMIL-100 (Fe)	H_3BTC	1.24	RB 68.69	Pseudo second-order kinetic model	Langmuir isotherm	Electrostatic interaction, hydrogen bonding	[28]
Cu-BTC	H_3BTC	279	MB 200	Pseudo second-order kinetic model	Langmuir isotherm	Electrostatic forces, π-π interactions, hydrogen bonding	[29]
Mn-BTB	H3BTB	5.089	MB 62.5	Pseudo second-order kinetic model	Langmuir isotherm	Electrostatic interaction, π-π interaction	[30]
TMU-7	H_2oba and the 4-bpdh	393	CR 79	Pseudo first-order kinetic model	Langmuir isotherm	Electrostatic interaction, π-π interaction	[31]
TMU-39	H_2oba	521	CR 53	Pseudo second-order kinetic model	Langmuir isotherm	Electrostatic interaction, π-π interaction	[32]
Cd-based MOF	INA and ISB	384	MO 166.7	Pseudo second-order kinetic model	Langmuir isotherm	Electrostatic interaction	[33]
Al-based MOF	succinic acid	117.6	AO7 559.28	Pseudo second-order kinetic model	Langmuir isotherm	Electrostatic interaction, hydrogen bonding	[34]
2D BUC-17	tib	2.39	CR 4923.7	Pseudo second-order kinetic model	Langmuir isotherm	Electrostatic interaction, ion-exchange, hydrogen-bonding, π-π interaction	[45]
2D Cu(II)–$5N_3IP$	H_25N_3IP		MB > CR > RhB > MO			Hydrogen-bonding, π-π interaction	[46]
2D Ni-based MOF	D-H_2cam and bpzpip	18	MB 185.5	Pseudo second-order kinetic model	Langmuir isotherm	Electrostatic interaction, π-π interaction	[47]
2D Zn-based MOF	H_3BTC and L		RhB 24.36 MB 21.55			Electrostatic interaction, hydrogen-bonding	[48]
2D Zn-based MOF	H_4L		MB 139.6 MO 116.9			Electrostatic interaction, π-π interaction	[49]
2D Cd-based MOF	$L(NH_2)_2$ and $ipaH_2$		CV 221			Electrostatic interaction, π-π interaction, Lewis acid-base interaction	[50]
3D Zn-based MOF	OH-bim and D-H_2Cam	Sqp topology				Electrostatic interaction, π-π interaction	[61]

3D FJI-H-U1	H_4TCPE	Tbo topology	EV 78.2% RB 63.3%			Electrostatic interaction, ion-exchange	[62]
3D JLU-Liu 39	H_2L	Fjh topology	MB 308 MV 84			Electrostatic interaction, ion-exchange	[63]
3D Co-based MOF	H_2BPDC and biimb	Hxl topology	MO 53.3	Pseudo second-order kinetic model	Langmuir isotherm	Electrostatic interaction, π-π interaction	[65]
3D Cu-based MOF	1,4-H_2ndc and L	Pcu topology	MB 7.34			Electrostatic interaction, π-π interaction	[66]
3D Co-based MOF	H_2oba and bpe	α-Po topology	MO 61.67			π-π interactions, hydrogen bonding	[68]
3D Cd-based MOF	Ppada and abpy	Sql topology	MB 315.2			Electrostatic interaction	[69]
3D Zn-based MOF	H_3BTB and bbis	Ins topology	MB 348			Electrostatic interaction	[70]
Modified MOFs as dye adsorbent - on the basis of metal node functionalization							
ZIF-8	2-methylimidazole	1380	RDB 133.76	Pseudo second-order kinetic model	Langmuir isotherm	Electrastatic interatio, π-π interaction, the hydrophobic bonds	[78]
Fe/ZIF-8		1243	RDB 193.56				
Ni-BTC	H_3BTC	1156	CR 828.50	Pseudo second-order kinetic model	Langmuir isotherm	Electrostatic interation, π-π interaction, hydrogen bonding	[85]
Ni-Cu BTC		1062	CR 999.20				
Ni-BTC	H_3BTC	15.4	MB 765.5	Pseudo second-order kinetic model	Langmuir isotherm	Electrostatic interation, π-π interaction, hydrogen bonding	[86]
Ni-Cu BTC		1450					
UiO-66	H_2BDC	1358	CR 251	Pseudo second-order kinetic model	Langmuir isotherm	Electrostatic interaction	[87]
Ti-UiO-66		792	CR 979				
UiO-66	H_2BDC	981	MB 24.5 MO 172.5	Pseudo second-order kinetic model	Langmuir isotherm	π-π interaction	[88]
Ce-UiO-66		1135	MB 145.3 MO 639.6				
Modified MOFs as dye adsorbent - on the basis of linker functionalization							
MIL-125	H_2BDC	470	MB 321.39	Presudo-second order model	Langmuir isotherm	Electrostatic interaction π-π interaction	[90]
NH_2-MIL-125	NH_2-H_2BDC	1028	MB 405.61				
MIL-125	H_2BDC	499				Electrostatic interaction π-π interaction, hydrogen bonding	[91]
NH_2-MIL-125	NH_2-H_2BDC	1350	BB 41 1257 MB 862				

UiO-66	H_2BDC	873.21	MB 90.98	Presudo-second order model	Langmuir isotherm	Electrostatic interaction	[92]
UiO-66-NH_2		616.55	MB 96.45				
TMU-16	H_2BDC and 4-bpdh		MO 350	Presudo-second order model	Langmuir isotherm	Electrostatic interaction, hydrogen bonding	[93]
TMU-16-NH_2	NH_2-H_2BDC and 4-bpdh		MO 393.7				
MIL-101 (Al)	H_2BDC		MB 195	Presudo-second order model	Langmuir isotherm	Electrostatic interaction, Lewis acid-base interaction	[94]
NH_2-MIL-101 (Al)	NH_2-H_2BDC	1980	MB 762				
ZJU-24	H_4TPTC and H_6TPHC	2316				Electrostatic interaction	[98]
ZJU-24-COOH		1189	MB 902				
MIL-101	H_3BTC	3016	FS 297.5			Electrostatic interaction, ion exchange	[99]
MIL-101-SO_3H	2-sulfoterephthalic acid	1546	FS 422.5				
MIL-101	H_3BTC	4100		Presudo-second order model	Langmuir isotherm	Electrostatic interaction	[100]
MIL-101-SO_3H	2-sulfoterephthalic acid	1411	MB 351 MG 351				
Defective MOFs as dye adsorbent							
UiO-66	H_2BDC	851	MB 73.5	Presudo-second order model		Electrostatic interaction, the exposure of hydrogen ions,	[103]
UiO-66-acetic acid	H_2BDC and Acetic acid	1090	MB 101			Missing-linker defects	
UiO-66	H_2BDC	980	DCM 510.3	Presudo-second order model	Langmuir-Freundlich (L-F)	Missing-linker defects	[104]
UiO-66-acetic acid	H_2BDC and acetic acid	1470	DCM 346.4		isotherm		
MIL-101	H_2BDC	1133.7				Missing-linker defects	[107]
MIL-101-formic acid	H_2BDC and formic acid	2688.5					
UiO-66	H_2BDC	1200	ST 39			Missing-linker defects, size-exclusion effect	[108]
UiO-66-benzoic acid	H_2BDC and benzoic acid	1890	ST 366				
UiO-66	H_2BDC	1270	UiO-66 < BA-UiO-66 <			Missing-linker defects	[110]
UiO-66-benzoic acid	H_2BDC and benzoic acid	1759	FA-UiO-66				
UiO-66-formic acid	H_2BDC and formic acid	1496					

4. Defective MOFs as dye adsorbents

Defect engineering has arisen a promising strategy to adjust and optimize the structure of MOFs for better adsorption performance [101]. Defect is equal to structural disorder and heterogeneity, which within MOFs breaks the regular arrangement of atoms as well as the surface properties of the resulting materials [102]. Several approaches were proposed to introduce defects in MOFs: (a) acid modulators; (b) the postsynthetic treatment of MOFs with inoragnic acids; (c) the mixed-linker approach. Acetic acid modulated UiO-66 for highly selective adsorption property was attributed to more positive Zeta potential and enlarged surface area from 851 to 1090 m^2/g, where the adsorption capacity of MO (84.8 mg/g) was higher than that of acid-free UiO-66 (70.4 mg/g) [103]. Acetic acid played the same role in the acid modulated strategy of UiO-66 for enhanced dichloromethane adsorption capacity attributed to the missing linker defect, which could be confirmed by the surface area changed from 980 to 1470 m^2/g [104]. The good consequence of the missing-linkers equivalent to structural 'imperfection' is the expansive porosity [105]. On the other hand, the adsortion performance was affected by acetic acid considering the nucleation and the crysal growth rates [106].

Formic acid is an effective monocarboxylic acid as an additive. The MIL-101 (Cr) crystals with better-defined shape, higher surface area, larger pore volumn and better adsorption performance were found to be formed from reations with higher molar ratio of fomic acid/ $CrCl_3$ [107]. The comparation of two defective UiO-66 created by bezoic acid modulator treatment and HCl postsynthetic treatment was reported. Missing-linker effect contributed to expanded porosity and specific surface area, which is important to improve the adsorption selectivity for Safranine T (ST) over CV [108]. During the synthesis, the combiantion of trifluoroacetic and HCl contributed to a highly crystalline material, which was related to the increased adorption property [109]. Notably, the defective strategy offered increased surface area and expanded pore size at the no expense of chemcial stability [110]. Fig. 3 summarized the changed

BET surface area of the MOFs-modulator, mainly acetic acid, formic acid and benzoic acid. In addition, missing-linker defects created by acid modultor make MOF more hydrophilic, providing infinite possibilities for the adsorption of dye [111]. Lastly, defective MOFs based on a mixed-linker approach have been reported in the founding of Bueken et al. Defects created by the pyrolyzation of thermolabile linker in the the combination of a thermostable linker 1,4-benzenedicar-boxylate (bdc) with a thermolabile linker trans-1,4-cyclohexanedicarboxylate (cdc). The UiO-66 structure is shown to tolerate up to 4.3 missing linker defects per $[Zr_6O_4(OH)_4]^{12+}$ node, with higher defect densities compromising the framework's structural integrity and porosity [112]. In addition, characterization and quantification of defects is also a difficult task, in the work of Shearer et al., four quantification "defectivity descriptors" including PXRD, nitrogen adsorption, dissolution/NMR and TGA data was used to locate and quantify defects, in addition, the combination with computational chemistry offers more possibilities for solving puzzles [113].

5. Composite MOFs as dye adsorbents

5.1 On the basis of carbon material

As a new highly porous crystalline material, MOFs has been widely used in dye absorption, and the open framework, the large number of void spaces as well as instability restric the adsorption performance, however, the combination MOFs with other substrates on account of the increased adsorption sites and improved stability is worthy of attention. Compare to ZIF-8@CNT (carbon nanotubes) (2034 mg/g), ZIF-8@GO (graphene oxide) exhibited improved adsorption capacity (3300 mg/g) [114]. Since the concept of MOF/GO nanocomposites have been developed, there are many reports on their applications in dye adsorption [115,116].

A Ni-MOF/GO (TMU-5/GO) as adsorbent for CR (2789 mg/g) was successfully synthesized by ultrasonic wave-assisted ball milling. The pseudo-second-order kinetic model and Freundlich adsorption isotherm model were used to describe the adsorption behavior. The greater amount of adsorbed CR was derived from the electrostatic

interaction and acid-base interaction [117]. Besides, compared to Ni-MOF/GO, RGO/NH_2-MIL-68 (Al) have a similar adsorption performance on CR (473.93 mg/g) [118]. Ni-MOF/GO exhibited adsorption performance not only on CR but also on MB [119]. The adsorption of MB on a HKUST-1/GO was estimated to 183.4 mg/g, and increased surface area and pore volume derived from the incorporation of GO as well as decreased pore size contributed to the excellent performance [120]. Compare to the parent materials, GO-TMU-23 nanocomposite synthesized by sonochemical route made the adsorption kinetics for MB accelerated [121]. Sonochemical synthesis was also applied for the preparation of GO-TMU-16. Various adsorption mechanisms were responsible for the adsorption process, including the electrostatic, physical adsorption and π-π interaction [122].

The introduction of UiO-67 nanoparticles into GO sheets exhibited improved adsorption capacity for glyphosate (482.69 mg/g) on the account of the abundant Zr-OH groups and adsorption sites created by GO [123]. Solvothermally prepared MIL-68(In)-NH2@GO composites as a presentative of In-based MOF was effective for the RhB asdorption. Both π-π interaction and the negative charge in the GO sheets co-contributed to the adsorption process [124]. The adsorption property of MOF-5@GO composite prepared by a solvothermal synthesis route was also confirmed [125].

Recently, zeolitic imidazolate (ZIF-8) based on 2D GO and carbon nanotubes (CNTs) as adsorbents for removal of MG were compared. ZIF-8@CNT existed in the form of aggregates, however, ZIF-8 was well dispersed by GO for higher surface area and pore volume [126]. ZIF-67- aerogel homo -dispersed on a 3D rGO was prepared via in situ assembly method, not only providing synergistic effects, but also conductive to separation. The porous composites exhibited superior adsorption capacity for MO (426.3 mg/g) and CV (1714.2 mg/g), which was mainly drive by π-π interactions, electrostatic interactions as well as synergistic effect [127].

Carbon nitride (g-C_3N_4) as graphene-like two-dimensional functional material, has attracted an intense interest by virtue of its unique nature, such as electrical, optical and adsorptive properties [128]. The combination g-C_3N_4 and MOFs played an important role in improving mechenical and thermodynamic stability. The activity of the g-C_3N_4 (20 wt%)/MIL-53(Al) composites is five times more effective than that of g-C_3N_4, which derived from favorable transport conditions due to increased specific surface area and pore volume [129]. Similarly, MIL-101 (Cr) showed better adsorption performance because of the g-C_3N_4 doping. The MIL-101 (Cr) exhibits S_{BET} of 4252 m^2 g^{-1} and Vp=2.9 cm^3 g^{-1}, however, which decreased to 837 m^2 g^{-1} and 0.4 cm^3 g^{-1} after g-C_3N_4 incorporation. Similar changes have occurred in the g-C_3N_4/MIL-53 (Fe) [130]. However, the porous structure parameters are in close between MIL-101 (Cr) and g-C_3N_4/MIL-101 (Cr), because of the new crystallization sites provided by g-C_3N_4 into the MIL-101. This difference in efficacy is mainly due to the newly added amino groups in nanocomposites [131]. In addition, Ni-Zn MOF/g-C_3N_4 nanoflowers (MG NFs) acted as an ideal solid-phase microextractent beacause of its advantages of abundant adsoption sites, large mesopore, excellent moisture and thermal stability [132]. Due to sensitivity of MOFs to water, improving the stability of MOFs and resistant to water by g-C_3N_4 doping are effective strategies. To improve the stability of Zn MOF nanoflowers, g-C_3N_4 and Ni were introduced to protect it from water corrosion [133]. Not only g-C_3N_4/MIL, but also g-C_3N_4/UiO have adsorptive property, such as g-C_3N_4/UiO-66 nanohybrids exhibited an adsorption effect on RhB [134]. A similar effect of g-C_3N_4/UiO-66 prepared by a facile annealing method could be applied to MB.

5.2 On the basis of metal nanoparticles

The practical application of MOFs materails was limited by the difficulty of separation and reuse, except for high speed centrifugation. The combination MOFs with magnetic metal nanoparticles could magnetize MOFs, especially, the composite materials with core-shell structure, higher stability and increased specific surface area

would be an excellent adsorbent [135,136]. A recyclable Fe_3O_4/Cu-MOFs composite was designed for adsorption of MB controlled by physical adsorption (344 mg/g) [137]. When changed to malachite green (MG), the adsorption capacities were found to be 113.67 mg/g [138]. By tuning the pore size to match dye molecules, both the enhanced selectivity and permeability properties of magnetic MOFs are able to realize. A novel type of Fe_3O_4@MOF matching the adsorbate would be an excellent adsorbent for the decoloration of MO (738.8 mg/g) [139]. Core-shell Fe_3O_4@MIL-100 (Fe) was designed by coverting MOFs shell onto core Fe_3O_4 nanoparticles through layer by layer method [140]. TEM images of Fe_3O_4 and Fe_3O_4@MIL-100 (Fe) nanoparticles by layer by layer method, notably, the MOF shell thickness of 21.4, 25 and 37.5 nm controlled by assembly cycles are shown in Fig. 4. Similar layer and layer methord was also applied to Fe_3O_4@MIL-100 (Fe) using Fe_3O_4@PAA nanoparticles as templates [141]. The advantage of this strategy is that the surface functional groups can be designed according to the ligand based on different adsorbates. Fe_3O_4@MIL-101 (Cr) was prepared by reducution-precipitation method to avoid the oxidation of Fe^{2+} is a valid adsorbent to remove the acid red 1(AR1) and orange G (OG) [142]. Another heterogeneous coprecipitation was applied for the assembly of Fe_3O_4@MIL-101(Fe), which had faster adsorption rate and higher adsorption capacity than MIL-101 [143]. In addition, Fe_3O_4@SiO_2 are often chosen as the core, based on it, the nano-sized Fe_3O_4@SiO_2 core (about 15 nm) was prepared with a shell of UiO-66 by means of in-situ growth [144]. In a similar study, amino-group functionalized Fe_3O_4@SiO_2 (Fe_3O_4@SiO_2-NH_2) was first synthesized, then the HKUST-1 grow by virtue of thr reaction between the amino group and carboxyl group. The composite features both magnetic separation characteristic and high porosity of MOF, making it an excellent adsorbent for removal of CR (49.5 mg/g) [145]. The synthetic route of Fe_3O_4@SiO_2-NH_2@HKUST-1 and Fe_3O_4@SiO_2@UiO-66 was shown in Fig.5.

The emergence of biological nanomaterials Fe_3O_4@MOFs with low ecological

toxicity brought good news for the treatment of dye wastewater. Bioadsorbent composed of chitosan (CS) wrapping nanascale Fe_3O_4 and MIL-101 exhibited excellent adsorption performance towards MO. Compared with pure MIL-101, the adsorption capacity of MO by CS/Fe_3O_4/MIL-101 was increased by 40%, however, which decreased with excessive Fe_3O_4 nanoparticles because of blocked pore [146]. The bacteria supported nontoxic core-shell Fe_3O_4@MIL-100 used as excellent biological decolorizer and the decolorization process fitted the second-order kinetics [147]. Thus, the combination of MOFs adsorbent and biotechnology could offer greater possibilities for the pollutant removal.

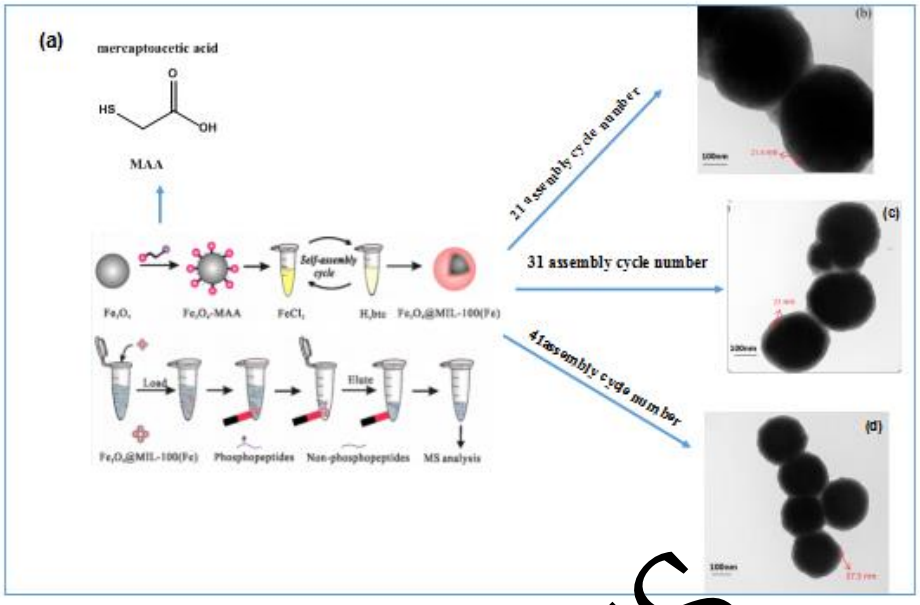

Fig.4 (a) Core-shell Fe_3O_4@mil-100 (Fe) prepared by layer by layer method. TEM images of core-shell magnetic nanoparticles of Fe_3O_4@MIL-100 (Fe) with (b) 21, (c) 31, and (d) 41 assembly cycles. (reprinted with permission from ref.141. Copyright (2015). American Chemical Society).

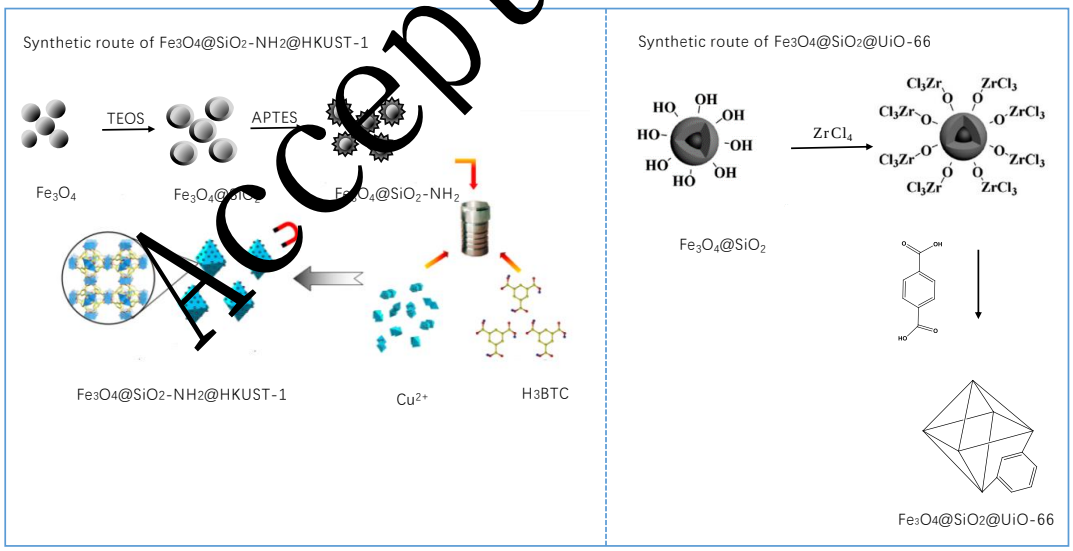

Fig.5 The comparation of sythetic route of Fe_3O_4@SiO_2-NH_2@HKUST-1 and Fe_3O_4@SiO2@UiO-66 (reprinted with permission from ref.144 and 145. Copyright (2018 and 2015). Elsevier and the Royal Society of Chemistry).

5.3 On the basis of polymolybdate (POMs)

POM-based MOFs composites with negative charges can be exclusive adsorption of cationic dyes [148]. A $[Ni_4(PPA)_4(H_2O)_6(b\text{-}Mo_8O_{26})]_8H_2O$ based on the pyridyl-amide-carboxylate ligand, 6-(pyridine-3-ylcarbamoyl) picolinic acid (HPPA) has been synthesized and used for the selective separation of MB (33.2 mg/g) [149]. Polyoxomatallate $H_6P_2W_{18}O_{62}$ played an important role in the $H_6P_2W_{18}O_{62}$/MOF-5 used for selective adsorption of cation dyes MB (51.81 mg/g) [150]. Polyoxometallate $H_6P_2Mo_{15}W_3O_{62}$ has a similar effect in the $H_6P_2Mo_{15}W_3O_{62}@Cu_3(BTC)_2$ on the selective adsorption of positively charged MB molecules rather than negatively charges MO [151]. Similarly, the thermodynamic data fitted the Langmuir model well representing the mono-layer adsorption. Other POM-MOFs composite adsorbents for the adsorption of MB included POM@MIL-101 [152], POM-MOF hybrid microporous material [153] and supramolecular hybrids $[SiW_{12}O_{40}]^{4-}$ @Co-based MOFs. Three supramolecular structural hybrids $[SiW_{12}O_{40}]^{4-}$ @Co-based MOFs were compared by changing the solvents [154]. Three $[SiW_{12}O_{40}]^{4-}$ @Co-based MOFs were prepared in the presence of H_2O, (1) EtOH/H_2O (2), DMA/H_2O (3), interestingly, (1) and (2) showed good adsorption activities for cationic dyes, however, the addition of DMA changes the surface charge of (3) for anionic dye CR.

6. Derived MOFs as dye adsorbents

MOFs have been applied as ideal templates to prepare various nanostructured materials, such as heteroatom-doped carbons, transition-metal oxides (TMOs), and transition-metal oxide-carbon (TMO@C) composites [155]. The MOF-derived nanostructures offer many unique advantages:1) designability of chemical composition by various MOFs; 2) expanded specific surface area and porosity; 3) low cost and easy synthesis.

A hierarchically porous carbon (HPC) was synthesized by pyrolysis and graphitization of template MOF-5 for enhanced adsorption of aromatic contaminants owing to the unique structure and π-π interaction [156]. MOF-1 as a precursor was

pyrolyzed at 1000 ℃ to obtain HPC which containing oxygen and nitrogen , was very competitive in the adsorption of PPCPs [157]. Porous carbons obtained from MAF-6 used as potential adsorbent for artificial sweeterners (ASWs) on account of their stability, high porosity, surface functionality, and hydrophobicity. The pyrolysis temperature was the main factor determined the adsorption process and 6h was considered as the most suitable time [158]. The ZIF-8 templated carbons prepared via polymerization of the ZIF-8 with furfuryl alcohol (FA) as additional carbon source also exhibited adsorption performance [159]. ZIF-8 was often selected as a precursor because of the sodalite-like structure, mild preparation condition and highly thermal stability [160]. However, the nanoporous carbons (NPC) derived from a one-step carbonization of ZIF-8 without carbon source could enrich ciprofloxacin (CIP) [161].

The carbonated ZIF-8 adsorbent at 1000 ℃ exhibited outstanding adsorption for MB (186.3 mg/g) compared to ZIF-8 (19.5 mg/g) [162]. Especially, some MOFs-derived carbon materials with specific structure were worthy of attention. The amount of CR reached 1600 mg/g by MOF-derived multi-walled carbon nanotubes (MWCNTs) [163]. 1D carbon nanorods and 2D graphene nanoribbons were prepared. Among them, 1D carbon nanorods were achieved by self-sacrificial and morphology-preserved thermal transformation of MOF-74. Based on the thermal activation of the solid carbon nanorods, the synthesis of the graphene nanoribbons with two- to six-layer thickness has also been accomplished by sonochemical treatment. The application of novel efficiency and high performance materials on supercapacitor electrodes has also been demonstrated, however, the adsorption application of them deserved attention [164].

Furthermore, the chemical properties of the porous carbon materials can be further treated by introducing heteroatoms, such as O, S and N. The porous carbon doping nitrogen through the carbonization of ZIF-8/urea composites was prepared and exhibited high adsorption property due to Lewis acid-base interaction, electrostatic and hydrogen bonding interaction [165]. The property of MOF-derived N,S-co-doped

563 nanocarbon is worthy of paying attention, which is synthesized by carbonization and
564 pore size design, then further co-coping sulfur to generate more active sites [166].

565 Owing to the metal ions coordinated with linker in the MOFs, the thermolysis of
566 MOFs can produce nanoscale materials with metal matrix [167]. Co-doped
567 hierarchically porous carbon (Co/HPC) was effective for the adsorption of MB
568 bccause uniformly dispersed Co nanoparticles confined in the nanopores [168].
569 Bimetallic Zn/Co ZIFs can also be chosen as a precursor to prepare porous carbon
570 doped by Co [169]. Ni doped porous carbon acted as adsorbents such as Ni@C and
571 Ni/PC-CNT [170,171].

572 In addition, metal oxide nanoparticles were also a class of derived MOFs
573 adsorbents. Compare to conventional methods, the MOFs-derived metal oxide has
574 various advantages. First, simple operation processes facilitate large-scale use. Second,
575 turned morphology, size, and elemental composition of the metal oxides were from
576 varied MOFs. Third, the porous structure of MOFs enables adsorption of other
577 precursors like mesoporous silica and molecular sieve. The CeO_2 nanofibers came
578 from calcination of Ce-BTC as a green adsorbent, and π-π interaction and electrostatic
579 interactions were responsible for the unideal adsorption capacity (86.6 mg/g) [172].
580 Further, NiO with excellent adsorbing capability was obtained by thermolysis of the
581 precursor at 350 °C [173]. The porous N-doped TiO_2-carbon nanotablets was prepared
582 via one-step solid-state thermolysis of NH_2-MIL-125(Ti), which inherited the
583 morphology of the template and kept the original nanoporous structure. Compared to
584 C_3N_4 and 3D graphene, the hierarchical meso/microporous structural resultant
585 composites showed remarkable adsorption ability [174].

Table 2. Recent progress in composite and derived MOFs as dye adsorbent

MOFs	S_{BET} (m^2/g)	Q_0 (mg/g)	Adsorption kinetics	Adsorption thermodynamics	Mechanism	References
Composite MOFs on the basis of carbon materials						
ZIF-8	1451.8	MG 1667	Pseudo-second-order kinetic model	Langmuir isotherm	π-π interaction	[114]
ZIF-8@GO	46.4	MG 2034				
ZIF-8@CNT	79.7	MG 3300				
Ni-MOF	59.8	CR 2489	Pseudo-second-order kinetic model	Freundlich adsorption isotherm	Lewis Acid-base interaction.	[117]
GO/Ni-MOF	69.6					
NH_2-MIL-68(Al)	1373	CR 473.93	Pseudo-second-order kinetic model	Langmuir isotherm	Electrostatic interaction, π-π interaction and hydrogen bonds	[118]
RGO/NH_2-MIL-68(Al)	1914					
Ni-MOF	16	MB 156	Pseudo-second-order kinetic model	Langmuir isotherm	Electrostatic interactionand acid–base interaction	[119]
GO/Ni-MOF	75	MB 274.3				
HKUST-1	575		Pseudo-second-order kinetic model	Langmuir isotherm	π-π interaction	[120]
GO/HKUST-1	1274	MB 183.49				
GO/TMU-23		MB 6.67	Pseudo-first order kinetic model		Electrostatic interaction, acid-base interactions, π-π interaction	[121]
MIL-68(In)-NH_2	526.8	RhB 66.8	Pseudo-second-order kinetic model	Langmuir isotherm	π-π interaction	[124]
GO/MIL-68(In)-NH_2	679.5					
ZIF-67	1470	CV 1714.2	Pseudo-first-order kinetic model		Electrostatic interaction,π-π interaction	[127]
rGO/ZIF-67	491	MO 426.3				
Composite MOFs on the basis of metal nanoparticles						
$Fe_3O_4/Cu_3(BTC)_2$	79.52	MB 84	Pseudo-second-order kinetic model	Frenudlich isotherm	π-π interaction, hydrogen bonding	[137]
$Fe_3O_4/Cu_3(BTC)_2$	35.4	MG 113.67	Pseudo-second-order kinetic model	Langmuir isotherm	Electrostatic interaction,physical adsorption	[138]

Fe_3O_4@MIL-100(Fe)	366.14	MB 738.8	Pseudo-first-order kinetic	Langmuir isotherm	Electrostatic interaction,π-π interaction	[139]
MIL-101	2263	MO 29.5	Pseudo-second-order kinetic model	Langmuir isotherm	Electrostatic interaction, π-π interaction	[141]
Fe_3O_4/MIL-101	3300	MO 80				
MIL-101	3312	AR1 83.3	Pseudo-second-order kinetic model	Langmuir isotherm	Coordination bonds, hydrogen bonds and π-π interaction	[142]
Fe_3O_4/MIL-101	1790	OG 133.3				
MIL-101	3420	MO 87.5	Pseudo-second-order kinetic model	Langmuir isotherm	π-π interaction, hydrogen bonding	[143]
Fe_3O_4/MIL-101	970	MO 117.6				
Fe_3O_4@SiO_2-NH_2@UiO-66	1044	MO 219	Pseudo-second-order kinetic model	Langmuir isotherm	π-π interaction, hydrogen bonding	[144]
HKUST-1	1316	CR 58.3	Pseudo-second-order kinetic model	Langmuir isotherm	Electrostatic interaction, π-π interaction	[145]
Fe_3O_4@SiO_2-NH_2@HKUST-1	1134	CR 49.5				
Composite MOFs on the basis of POMs						
MOF-5	92	MB26.75	Pseudo-second-order kinetic model	Langmuir isotherm	Electrostatic attraction	[149]
$H_6P_2W_{18}O_{62}$/MOF-5	395	MB 52.75				
$Cu_3(BTC)_2$	988	MB 77.22	Pseudo-second-order kinetic model	Langmuir isotherm	Electrostatic attraction	[150]
$H_6P2Mo_{15}W_3O_{62}$@$Cu_3(BTC)_2$	561					
POM@MIL-101	10	MB 371	Pseudo-second-order kinetic model	Langmuir isotherm	Electrostatic attraction	[151]
UiO-66	969	RhB 60	Pseudo-second-order kinetic model	Langmuir isotherm	Electrostatic attraction	[152]
POM@UiO-66	227	RhB 222.6				

586

587

Table 3. Recent progress in the derived MOFs as dye adsorbent

Derived MOFs	Template	Temperature（℃）	S_{BET} (m^2/g)	Q_0 (mg/g)	Adsorption kinetics	Adsorption thermodynamics	Adsorption Mechanism	References
HPC	MOF-5	950	1512	PNP 243.9	Pseudo-second-order kinetic model	Langmuir isotherm	Hierarchical pores and π－π interaction	[156]
BMDCs	MOF-1	1000	1449	ATNL 552	Pseudo-second-order kinetic model	Langmuir isotherm	Electrostatic attraction	[157]
MDC	ZIF-8	1000	1525	ASWs 93		Langmuir isotherm	Hydrogen bonding	[158]
MDC	ZIF-8	1050	1069	H2 6.2 wt%				[159]
NPC	ZIF-8	700	750	CIP 416.7	Pseudo-second-order kinetic model	Freundlich isotherm	Electrostatic attraction	[161]
NPC	ZIF-8	1000	1043.1	MB186.3	Pseudo-second-order kinetic model	Langmuir isotherm	Electrostatic attraction	[162]
MWCNTs	Co-based MOF	800	52.07	CR 1639			Electrostatic attraction, π－π interaction, hydrogen bonding	[163]
Carbon-ZD	ZIF-8	950	1796.5	MB 1160.5	Pseudo-second-order kinetic model	Langmuir isotherm	Electrostatic attraction, nitrogen doping	[164]
Co/NPC	ZIF-67	800	345	MB 502.5	Pseudo-second-order kinetic model	Langmuir isotherm	π－π interaction	[168]
HPC	Zn/Co ZIFs	900	398.7	RhB 1162	Pseudo second-order kinetic model	Langmuir isotherm	Electrostatic attraction	[169]
Ni@C	Ni-based MOF	420	120.382	MB 84.5			Electrostatic attraction, surface defects interction	[170]
Ni/PC-CNT	Ni/Zn-MOF	910	999	MG 898 MB 271	Pseudo second-order kinetic model	Langmuir isotherm	π－π interaction, hydrogen bonding	[171]

7. **Conclusions and future challenges**

In summary, we provide a comprehensive review of recent developments in MOFs and MOF-based materials for the adsorption of dyes. The metal node and ligand played an equally important role in constructing MOFs-based materials take advantage of high surface, tunable porosity and stability. The selection and seembly of metal center and ligand endows MOFs with infinite possiblity and charm.

(1) Multidimensional MOFs take the advantage of adjustable structure with large specific surface area and stability have attracted attention. Especially, two dimensional nanosheet and MOFs thin film showed excellent adsorption, there is still a long way to expand its application in dye adsorption.

(2) Mixed-metal modification is an effective strategy to improve the adsorption capacity, however, it is a difficult problem of the localization and quantification of mixed-metal. In addition, most studies have linked increased adsorption capacity to more active sites and related mechanism remain to be revealed.

(3) Based on mixed ligand strategy and secondary building units, abudant MOFs offers unlimited possibilities for dye adsorption. At the present stage, most studies focused on the rigid ligands, however, the combination of flexible and rigid ligand is more outstanding in terms of solid stability and adsorption performance. In addition, functional ligands focused on amino modified ligands, more functional groups modified ligands need attention.

(4) Defect design is a good strategy to improve adsorption capacity and characterization and quantification of which are essential to improve adsorpt capacity. A combinaiton of characterization and computational chemisty is essensial to reveal the defect secrets.

(5) The separability and reusability are also indicators to consider materials. It is necessary for adsorbent to endow the MOFs magnetism for separation.

(6) The study of porous carbons are mainly in electrochemical field, it will be a good option to apply them for dye adsorption.

8. Acknowledgements

This study was financially supported by the Program for the National Natural Science Foundation of China (51879101, 51579098, 51779090, 51709101, 51521006, 51809090, 51278176, 51378190), the National Program for Support of Top－Notch Young Professionals of China (2014), the Program for Changjiang Scholars and Innovative Research Team in University (IRT-13R17), and Hunan Provincial Science and Technology Plan Project (2018SK20410, 2017SK2243, 2016RS3026), and the Fundamental Research Funds for the Central Universities (531109200027, 531107051080, 531107050978).

Abbreviation			
Dye			
AB 92	Acid Blue 92	BB 41	Basic Blue 41
BR9	Basic Red 9	BR 46	Basic Red 46
BV 14	Basic violet 14	DR 80	Direc red 80
CR	Congo Red	CV	Crystal violet
MR	Methyl Red	MV	Methyl violet
MB	Methyl blue	MO	Methyl Orange
RhB	Rhodamine B	RDB	Remazol Deep Black
ST	Safranine	EV	Ethyl Violet
Ligand			
abpy	4,4’-azobis(pyridine)	bdc	1,4-benzennedicar-boxylate
bpzpip	N,N’-bis(pyraz-2-yl)piperazine	btc	Benzene-tricarboxylates
cdc	Trans-1,4-cyclohexanedicarboxylate	D-camH_2	Camphoric acid
FA	Fumaric acid	H_2oba	4,4’-oxybis)benzoic acid
HF	Hydrpfluoric acid	H_3BTB	1,3,5-tris(4-carboxyphenyl)benzene
H_2IP	Isophthalic acid	H_4TCPE	Tetrakis (4-carboxyphenyl)ethylene
H_2BPDC	Biphenyl-4,4’-dicarboxylic acd	H_2L	Pyridine-3,5-bis(phenyl-4-carboxylic acid)
ISB	Isobutanol	INA	Isonicotinate
L	1,4-bis(4-pyridyl)-2,3-diaza-1,3-butadiene	OH-bim	2-(1-hydroxyethyl)benzimidazole
pdc	Pyridine-2,3-dicarboxylate	ppda	1,4-phenylenediacetate
tib	1,3,5-tris(1-imidazolyl)benzene	SA	Succinic acid
btaH$_4$	4,4’,4”,4”’-([1,1’-biphenyl]-3,3’,5,5’-tetrayl)tetrakis(ethyne-2,1-diyl) tetrabenzoic acid		
ptbaH$_4$	4,4’,4”,4”’-(pyrene-1,3,6,8-tetrayl)tetrakis-(ethyne-2,1-diyl)tetrabenzoic acid		
MOFs			
BUC-17	$[Co_3(tib)_2(H_2O)_{12}](SO_4)_3$	BUC-60	$Co(tib)(ADC)_2$
BUC-61	$Zn_3(tib)_2Cl_6$	BUC-62	$[Cu_2(tib)_2(MoO_4)Cl]Cl$
TMU-7	[Cd(oba)(4-bpdh)]$_n$ 1DMF	TMU-16	$[Zn_2(BDC)_2(4\text{-bpdh})]$ 3DMF
TMU-39	$[Zn_4(oba)_3(DMF)_2]$	TMU-23	$[Zn_2(oba)_2(bpfb)]$ $(DMF)_5$
JLU-Liu18	$[NO_3][In_3OL_3]$ 4DMF $3H_2O$	JLU-Liu39	$[(CH_3)_2NH_2]_2[Cu_3O(SO_4)_3Cu_2L_2(DMF)(H_2O)]$ 9DMF
Fe-ZIF-8	Iron-doped ZIF-8	HKUST-1	$Cu_3(BTC)_2$
ZIF-8	zeolitic imidazolate	PL-MOFs	3D pillared-layer MOFs
Others			
0D	Zero-dimensional	1D	One-dimensional
2D	Two-dimensional	3D	Three-dimensional
ASWs	Artificial sweeteners	CNT	Carbon nanotubes
CIP	Ciprofloxacin	FA	Furfuryl alcohol
GO	Graphene oxide	HPC	Hierachically
HF	Hydrpfluoric acid	M-N	Metal to nitrogen
NPC	Nanoporous carbons	MWCNTs	Multi-walled carbon nanotubes

TMOs	Transition-metal oxides	SBUs	Secondary building units
XANES	Xray absorption near edge structure	XRD	X-ray diffraction
AC	Activated carbon		

636

9. References

[1] G. Zeng, M. Chen, Z. Zeng, Science, 340 (2013) 1403.

[2] S.-F. Yang, C.-G. Niu, D.-W. Huang, H. Zhang, C. Liang, G.-M. Zeng, Environmental Science: Nano, 4 (2017) 585-595.

[3] J.-H. Deng, X.-R. Zhang, G.-M. Zeng, J.-L. Gong, Q.-Y. Niu, J. Liang, Chemical Engineering Journal, 226 (2013) 189-200.

[4] X. Ren, G. Zeng, L. Tang, J. Wang, J. Wan, Y. Liu, J. Yu, H. Yi, S. Ye, R. Deng, The Science of the total environment, 610-611 (2018) 1154-1163.

[5] M. Cheng, G. Zeng, D. Huang, C. Lai, P. Xu, C. Zhang, Y. Liu, Chemical Engineering Journal, 284 (2016) 582-598.

[6] P. Xu, G.M. Zeng, D.L. Huang, C. Lai, M.H. Zhao, Z. Wei, N.J. Li, C. Huang, G.X. Xie, Chemical Engineering Journal, 203 (2012) 423-431.

[7] C. Zhang, C. Lai, G. Zeng, D. Huang, C. Yang, Y. Wang, Y. Zhou, M. Cheng, Water research, 95 (2016) 103-112.

[8] L. Qin, G. Zeng, C. Lai, D. Huang, P. Xu, C. Zhang, M. Cheng, X. Liu, S. Liu, B. Li, H. Yi, Coordination Chemistry Reviews, 359 (2018) 1-31.

[9] M. Sindoro, N. Yanai, A.Y. Jee, S. Granick, Acc Chem Res, 47 (2014) 459-469.

[10] H.-Y. Guan, R.J. LeBlanc, S.-Y. Xie, Y. Yue, Coordination Chemistry Reviews, 369 (2018) 76-90

[11] S. Li, Y. Chen, X. Fei, S. Zhang, X. Feng, J. Zhou, B. Wang, Chinese Journal of Chemistry, 34 (2016) 175-185.

[12] J. Wen, Y. Fang, G. Zeng, Chemosphere, 201 (2018) 627.

[13] M. Feng, P. Zhang, H.C. Zhou, V.K. Sharma, Chemosphere, 209 (2018) 783-800.

[14] J. Li, X. Wang, G. Zhao, C. Chen, Z. Chai, A. Alsaedi, T. Hayat, X. Wang, Chemical Society reviews, 47 (2018) 2322-2356.

[15] A. Samokhvalov, Chemistry, 21 (2015) 16726-16742.

[16] C. Liu, L.Q. Yu, Y.T. Zhao, Y.K. Lv, Mikrochimica acta, 185 (2018) 342.

[17] A. Ayati, M.N. Shahrak, B. Tanhaei, M. Sillanpaa, Chemosphere, 160 (2016) 30-44.

[18] Z. Hasan, S.H. Jhung, Journal of hazardous materials, 283 (2015) 329-339.

[19] M. Cheng, C. Lai, Y. Liu, G. Zeng, D. Huang, C. Zhang, L. Qin, L. Hu, C. Zhou, W. Xiong, Coordination Chemistry Reviews, 368 (2018) 80-92.

[20] J. Li, X. Wang, G. Zhao, C. Chen, Z. Chai, A. Alsaedi, T. Hayat, X. Wang, Chemical Society reviews, 47 (2018) 2322-2356.

[21] D. Wang, F. Jia, H. Wang, F. Chen, Y. Fang, W. Dong, G. Zeng, X. Li, Q. Yang, X. Yuan, Journal of colloid and interface science, 519 (2018) 273-284.

[22] W. Xiong, G. Zeng, Z. Yang, Y. Zhou, C. Zhang, M. Cheng, Y. Liu, L. Hu, J. Wan, C. Zhou, R. Xu, X. Li, The Science of the total environment, 627 (2018) 235-244.

[23] L. Jiang, X. Yuan, Y. Pan, J. Liang, G. Zeng, Z. Wu, H. Wang, Applied Catalysis B: Environmental, 217 (2017) 388-406.

[24] E. Haque, J.W. Jun, S.H. Jhung, Journal of hazardous materials, 185 (2011) 507-511.

[25] E. Yılmaz, E. Sert, F.S. Atalay, Journal of the Taiwan Institute of Chemical Engineers, 65 (2016) 323-330.

[26] M. Tong, D. Liu, Q. Yang, S. Devautour-Vinot, G. Maurin, C. Zhong, Journal of Materials Chemistry A, 1 (2013) 8534.

[27] S.-H. Huo, X.-P. Yan, Journal of Materials Chemistry, 22 (2012) 7449

[28] S. Duan, J. Li, X. Liu, X. Wang, S. Zeng, D. Shao, T. Hayat, ACS Sustainable Chemistry & Engineering, 4 (2016) 3368-3378.

[29] S. Lin, Z. Song, G. Che, A. Ren, P. Li, C. Liu, J. Zhang, Microporous and Mesoporous Materials, 193 (2014) 27-34.

[30] J. He, J. Li, W. Du, Q. Han, Z. Wang, M. Li, Journal of Alloys and Compounds, 750 (2018) 360-367.

[31] M.Y. Masoomi, M. Bagheri, A. Morsali, Ultrasonics sonochemistry, 37 (2017) 244-250.

[32] N. Abdollahi, M.Y. Masoomi, A. Morsali, P.C. Junk, J. Wang, Ultrasonics sonochemistry, 45 (2018) 50-56.

[33] A.C. Tella, M.D. Olawale, M. Neuburger, J.A. Obaleye, Journal of Solid State

Chemistry, 255 (2017) 157-166.

[34] K.-W. Jung, B.H. Choi, C.M. Dao, Y.J. Lee, J.-W. Choi, K.-H. Ahn, S.-H. Lee, Journal of Industrial and Engineering Chemistry, 59 (2018) 149-159.

[35] C. Ni, G. Hedley, J. Payne, V. Svrcek, C. McDonald, L.K. Jagadamma, P. Edwards, R. Martin, G. Jain, D. Carolan, D. Mariotti, P. Maguire, I. Samuel, J. Irvine, Nature communications, 8 (2017) 170.

[36] Q. Zhang, E. Uchaker, S.L. Candelaria, G. Cao, Chemical Society reviews, 42 (2013) 3127-3171.

[37] W.L. Leong, J.J. Vittal, Chemical reviews, 111 (2011) 688-764.

[38] S. Mendiratta, M. Usman, K.-L. Lu, Coordination Chemistry Reviews, 360 (2018) 77-91.

[39] R. Mas-Balleste, C. Gomez-Navarro, J. Gomez-Herrero, F. Zamora, Nanoscale, 3 (2011) 20-30.

[40] O. Shekhah, J. Liu, R.A. Fischer, C. Woll, Chemical Society reviews, 40 (2011) 1081-1106.

[41] D.R.X. Dr, E.B.W. Prof, H.Y.A. Dr, Y.G.L. Dr, Z.M. Su, C.Y. Sun, Chemistry - A European Journal, 12 (2006) 6528–6541.

[42] Y. Wen, T. Sheng, Z. Sun, Z. Xue, Y. Wang, Y. Wang, S. Hu, X. Ma, X. Wu, Chemical communications, 50 (2014) 8320-8323.

[43] C.X. Bezuidenhout, V.J. Smith, C. Esterhuysen, L.J. Barbour, Journal of the American Chemical Society, 139 (2017).

[44] J.J. Li, C.C. Wang, H.F. Fu, J.R. Cui, P. Xu, J. Guo, J.R. Li, Dalton transactions, 46 (2017) 10197-10201.

[45] N. Ahmad, H.A. Younus, A.H. Chughtai, K. Van Hecke, Z.A.K. Khattak, Z. Gaoke, M. Danish, F. Verpoort, Catalysis Science & Technology, 8 (2018) 4010-4017.

[46] Y. Zhou, S. Yao, Y. Ma, G. Li, Q. Huo, Y. Liu, Chemical communications, 54 (2018) 3006-3009.

[47] M.-J. Tsai, J.-Y. Wu, Polymers, 9 (2017) 661.

[48] Y. Rachuri, S. Subhagan, B. Parmar, K.K. Bisht, E. Suresh, Dalton transactions, 47 (2018) 898-908

[49] J. Xu, Q. Zhuo, R. Fu, H. Cheng, X. Tang, Y. Ma, J. Xie, R. Yuan, Inorganica Chimica Acta, 446 (2016) 198-202.

[50] S. Chand, S.M. Elahi, A. Pal, M.C. Das, Dalton transactions, 46 (2017) 9901-9911.

[51] M. Zhao, Y. Huang, Y. Peng, Z. Huang, Q. Ma, H. Zhang, Chemical Society reviews, 47 (2018) 6267-6295.

[52] R. Sakamoto, K. Takada, X. Sun, T. Pal, T. Tsukamoto, E.J.H. Phua, A. Rapakousiou, K. Hoshiko, H. Nishihara, Coordination Chemistry Reviews, 320-321 (2016) 118-128.

[53] M. Zhao, Q. Lu, Q. Ma, H. Zhang, Small Methods, 1 (2017) 1600030.

[54]Y. Liu, X. Duan, Y. Huang, X. Duan, Chemical Society reviews, 47 (2018).

[55] W. Yang, Y. Peng, Y. Li, Y. Ban, Angew Chem Int Ed Engl, 56 (2017).

[56] Y. Peng, Y. Li, Y. Ban, H. Jin, W. Jiao, X. Liu, W. Yang, Science, 346 (2014) 1356.

[57] T. Rodenas, I. Luz, G. Prieto, B. Seoane, H. Miro, A. Corma, F. Kapteijn, I.X.F.X. Llabres, J. Gascon, Nature materials, 14 (2015) 48-55.

[58] S. Henke, A. Schneemann, A. Wutscher, R.A. Fischer, Journal of the American Chemical Society, 134 (2012) 9464-9474.

[59] N.C. Burtch, K.S. Walton, Acc Chem Res, 48 (2015) 2850-2857.

[60] K. Forrest, T. Pham, B. Space, Crystengcomm, 19 (2017).

[61] Y.H. Tang, F. Wang, J. Zhang, Dalton transactions, 47 (2018).

[62] F. Hu, Z. Di, P. Lin, P. Huang, M. Wu, F. Jiang, M. Hong, Crystal Growth & Design, 18 (2018) 576-580.

[63] S. Yao, T. Xu, N. Zhao, L. Zhang, Q. Huo, Y. Liu, Dalton transactions, 46 (2017).

[64] S. Yao, D. Wang, Y. Cao, G. Li, Q. Huo, Y. Liu, Journal of Materials Chemistry A, 3 (2015) 16627-16632.

[65] Y. Deng, Y. Zhao, P. Wang, Z.-Y. Yao, X.-D. Zhang, W.-Y. Sun, Microporous and

Mesoporous Materials, 241 (2017) 192-201.

[66] L. Yang, X. Li, C.-Y. Sun, H. Wu, C.-G. Wang, Z.-M. Su, New Journal of Chemistry, 41 (2017) 3661-3666.

[67] X.-L. Hu, F.-H. Liu, H.-N. Wang, C. Qin, C.-Y. Sun, Z.-M. Su, F.-C. Liu, J. Mater. Chem. A, 2 (2014) 14827-14834.

[68] S. Phengthaisong, A. Cheansirisomboon, J. Boonmak, S. Youngme, Inorganica Chimica Acta, 479 (2018) 172-178.

[69] G.G. Sezer, M. Arıcı, İ. Erucar, O.Z. Yeşilel, H.U. Özel, B.T. Gemici, H. Erer, Journal of Solid State Chemistry, 255 (2017) 89-96.

[70] M. Guo, S. Liu, H. Guo, Y. Sun, X. Guo, R. Deng, Dalton transactions, 46 (2017) 14988-14994.

[71] W.G. Jin, W. Chen, P.H. Xu, X.W. Lin, X.C. Huang, G.H. Chen, F. Lu, X.M. Chen, Chemistry, 23 (2017) 13058-13066.

[72] X.P. Wang, W.M. Chen, H. Qi, X.Y. Li, C. Rajnák, Z.Y. Feng, M. Kurmoo, R. Boca, C.J. Jia, C.H. Tung, D. Sun, Chemistry, 23 (2017) 7990-7996.

[73] L.H. Wee, M. Meledina, S. Turner, G. Van Tendeloo, K. Zhang, L.M. Rodriguez-Albelo, A. Masala, S. Bordiga, J. Jiang, J.A. Navarro, C.E. Kirschhock, J.A. Martens, Journal of the American Chemical Society, 139 (2017) 819-828.

[74] R. Sen, D. Saha, S. Koner, D. Mal, P. Brandão, Z. Lin, ChemPlusChem, 80 (2015) 591-598.

[75] J.-J. Li, C.-C. Wang, J. Guo, J.-R. Cui, P. Wang, C. Zhao, Polyhedron, 139 (2018) 89-97.

[76] J. Qiu, X. Zhang, Y. Feng, X. Zhang, H. Wang, J. Yao, Applied Catalysis B: Environmental, 231 (2018) 317-342.

[77] M.I. Breeze, G. Clet, B.C. Campo, A. Vimont, M. Daturi, J.M. Greneche, A.J. Dent, F. Millange, R.I. Walton, Inorganic chemistry, 52 (2013) 8171-8182.

[78] M.Thi Thanh, T. Vinh Thien, V. Thi Thanh Chau, P. Dinh Du, N. Phi Hung, D. Quang Khieu, Journal of Chemistry, 2017 (2017) 1-18.

[79] H. Yang, X.-W. He, F. Wang, Y. Kang, J. Zhang, Journal of Materials Chemistry,

22 (2012) 21849.

[80] F. Hillman, J.M. Zimmerman, S.M. Paek, M.R.A. Hamid, W.T. Lim, H.K. Jeong, Journal of Materials Chemistry A, 5 (2017) 6090.

[81] J. Sun, L. Semenchenko, W.T. Lim, M.F. Ballesteros Rivas, V. Varela-Guerrero, H.-K. Jeong, Microporous and Mesoporous Materials, 264 (2018) 35-42.

[82] J.A. Botas, G. Calleja, M. Sanchez-Sanchez, M.G. Orcajo, Langmuir : the ACS journal of surfaces and colloids, 26 (2010) 5300-5303.

[83] J. Liu, J. Zheng, D. Barpaga, S. Sabale, B. Arey, M.A. Derewinski, B.P. McGrail, R.K. Motkuri, European Journal of Inorganic Chemistry, 2018 (2018) 885-889.

[84] Y. Jiao, C.R. Morelock, N.C. Burtch, W.P. Mounfield, J.T. Hungerford, K.S. Walton, Industrial & Engineering Chemistry Research, 54 (2015) 12408-12414.

[85] J. Hu, H. Yu, W. Dai, X. Yan, X. Hu, H. Huang, RSC Adv., 4 (2014) 35124-35130.

[86] H.M. Abd El Salam, S.A. Younis, H.R. Ali, T. Zaki, Microporous and Mesoporous Materials, 241 (2017) 210-217.

[87] Y. Han, M. Liu, K. Li, Q. Sun, W. Zhang, C. Song, G. Zhang, Z.C. Zhang, X. Guo, Inorganic Chemistry Frontiers, 4 (2017).

[88] J.M. Yang, R.J. Ying, C.X. Han, Q.T. Hu, H.M. Xu, J.H. Li, Q. Wang, W. Zhang, Dalton transactions, 47 (2018) 3913-3920.

[89] S. Xing, Q. Ling, H. Qi, J. Liu, T. Bai, G. Li, Z. Shi, S. Feng, R. Xu, ACS applied materials & interfaces, 9 (2017) 23828-23835.

[90] R. Bibi, L. Wei, Q. Shen, W. Tian, O. Oderinde, N. Li, J. Zhou, Journal of Chemical & Engineering Data, 62 (2017) 1615-1622.

[91] M. Oveisi, M.A. Asli, N.M. Mahmoodi, Journal of hazardous materials, 347 (2018) 123-140.

[92] Q. Chen, Q. He, M. Lv, Y. Xu, H. Yang, X. Liu, F. Wei, Applied Surface Science, 327 (2015) 77-85.

[93] M. Roushani, Z. Saedi, T.M. Beygi, Journal of the Taiwan Institute of Chemical Engineers, 66 (2016) 164-171.

[94] E. Haque, V. Lo, A.I. Minett, A.T. Harris, T.L. Church, J. Mater. Chem. A, 2 (2014) 193-203.

[95] R. Bibi, L. Wei, Q. Shen, W. Tian, O. Oderinde, N. Li, J. Zhou, Journal of Chemical & Engineering Data, 62 (2017) 1615-1622.

[96] M. Oveisi, M.A. Asli, N.M. Mahmoodi, Journal of hazardous materials, 347 (2018) 123-140.

[97] Q. Zhang, J. Yu, J. Cai, R. Song, Y. Cui, Y. Yang, B. Chen, G. Qian, Chem. Commun., 50 (2014) 14455-14458.

[98] J.Y. Song, I. Ahmed, P.W. Seo, S.H. Jhung, ACS applied materials & interfaces, 8 (2016).

[99] X. Zhao, K. Wang, Z. Gao, H. Gao, Z. Xie, X. Du, H. Huang, Industrial & Engineering Chemistry Research, 56 (2017) 4496-4501.

[100] X.-P. Luo, S.-Y. Fu, Y.-M. Du, J.-Z. Guo, B. Li, Microporous and Mesoporous Materials, 237 (2017) 268-274.

[101] D.M. Driscoll, D. Troya, P.M. Usov, A.J. Maynes, A.J. Morris, J.R. Morris, The Journal of Physical Chemistry C, 122 (2018) 14582-14589.

[102] W. Liang, C.J. Coghlan, F. Ragon, M. Rubio-Martinez, D.M. D'Alessandro, R. Babarao, Dalton transactions, 45 (2016) 4496-4500.

[103] J. Qiu, Y. Feng, X. Zhang, M. Jia, J. Yao, Journal of colloid and interface science, 499 (2017) 151-158.

[104] L. Zhou, X. Zhang, Y. Chen, Materials Letters, 197 (2017) 167-170.

[105] H. Wu, Y.S. Chua, V. Krungleviciute, M. Tyagi, P. Chen, T. Yildirim, W. Zhou, Journal of the American Chemical Society, 135 (2013) 10525-10532.

[106] S. Hu, M. Liu, X. Guo, K. Li, Y. Han, C. Song, G. Zhang, Crystal Growth & Design, 17 (2017) 6586-6595.

[107] J. Ren, N.M. Musyoka, H.W. Langmi, T. Segakweng, B.C. North, M. Mathe, X. Kang, International Journal of Hydrogen Energy, 39 (2014) 12018-12023.

[108] K. Wang, C. Li, Y. Liang, T. Han, H. Huang, Q. Yang, D. Liu, C. Zhong, Chemical Engineering Journal, 289 (2016) 486-493.

[109] F. Vermoortele, B. Bueken, G. Le Bars, B. Van de Voorde, M. Vandichel, K. Houthoofd, A. Vimont, M. Daturi, M. Waroquier, V. Van Speybroeck, C. Kirschhock, D.E. De Vos, Journal of the American Chemical Society, 135 (2013) 11465-11468.

[110] P. Ghosh, Chemical communications, 50 (2014) 11329-11331.

[111] Y. Li, Y. Liu, W. Gao, L. Zhang, W. Liu, J. Lu, Z. Wang, Y.-J. Deng, CrystEngComm, 16 (2014) 7037-7042.

[112] B. Bueken, N. Van Velthoven, A. Krajnc, S. Smolders, F. Taulelle, C. Mellot-Draznieks, G. Mali, T.D. Bennett, D. De Vos, Chemistry of Materials, 29 (2017) 10478-10486.

[113] G.C. Shearer, S. Chavan, S. Bordiga, S. Svelle, U. Olsbye, K.P. Lillerud, Chemistry of Materials, 28 (2016) 3749-3761.

[114] J. Abdi, M. Vossoughi, N.M. Mahmoodi, I. Alemzadeh, Chemical Engineering Journal, 326 (2017) 1145-1158.

[115] P. Samaddar, Y.-S. Son, D.C.W. Tsang, K.-H. Kim, S. Kumar, Coordination Chemistry Reviews, 368 (2018) 93-114.

[116] J. Sosa, T. Bennett, K. Nelms, B. Liu, R. Liu, Crystals, 8 (2018) 325.

[117] S. Zhao, D. Chen, F. Wei, N. Chen, Z. Liang, Y. Luo, Ultrasonics sonochemistry, 39 (2017) 845-852.

[118] Z. Wu, X. Yuan, H. Zhong, H. Wang, L. Jiang, G. Zeng, H. Wang, Z. Liu, Y. Li, Journal of Molecular Liquids, 247 (2017).

[119] S. Zhao, D. Chen, F. Wei, N. Chen, Z. Liang, Y. Luo, Journal of Chemical Technology & Biotechnology, 93 (2018) 698-709.

[120] L. Li, X.L. Liu, H.Y. Geng, B. Hu, G.W. Song, Z.S. Xu, Journal of Materials Chemistry A, 1 (2013) 10292.

[121] M. Tanhaei, A.R. Mahjoub, V. Safarifard, Ultrasonics sonochemistry, 41 (2018) 189-195.

[122] M. Tanhaei, A.R. Mahjoub, V. Safarifard, Materials Letters, 227 (2018) 318-321.

[123] Q. Yang, J. Wang, W. Zhang, F. Liu, X. Yue, Y. Liu, M. Yang, Z. Li, J. Wang,

Chemical Engineering Journal, 313 (2017) 19-26.

[124]S. Zhao, D. Chen, F. Wei, N. Chen, Z. Liang, Y. Luo, Journal of Chemical Technology & Biotechnology, 93 (2018) 698-709.

[125] B.A. Crum, Yearbook of Neurology and Neurosurgery, 2009 (2009) 131-132.

[126] L. Asgharnejad, A. Abbasi, A. Shakeri, Microporous and Mesoporous Materials, 262 (2018) 227-234.

[127] Q. Yang, R. Lu, S.S. Ren, C. Chen, Z. Chen, X. Yang, Chemical Engineering Journal, (2018).

[128] H. Wang, X. Yuan, Y. Wu, G. Zeng, X. Chen, L. Leng, H. Li, Applied Catalysis B: Env`1ironmental, 174-175 (2015) 445-454.

[129] D. Guo, R. Wen, M. Liu, H. Guo, J. Chen, W. Weng, Applied Organometallic Chemistry, 29 (2015) 690–697.

[130] W. Huang, N. Liu, X. Zhang, M. Wu, L. Tang, Applied Surface Science, 425 (2017) 107-116.

[131] A. Argoub, R. Ghezini, C. Bachir, B. Boukoussa, A. Khelifa, A. Bengueddach, P.G. Weidler, R. Hamacha, Journal of Porous Materials, (2017) 1-7.

[132] N. Zhang, C. Huang, P. Tong, Z. Feng, X. Wu, L. Zhang, Journal of chromatography. A, 1556 (2018) 37-46.

[133] C. Zhou, C. Lai, D. Huang, G. Zeng, C. Zhang, M. Cheng, L. Hu, J. Wan, W. Xiong, M. Wen, X. Wen, L. Qin, Applied Catalysis B: Environmental, 220 (2018) 202-210.

[134] X. Zhang, Y. Yang, W. Huang, Y. Yang, Y. Wang, C. He, N. Liu, M. Wu, L. Tang, Materials Research Bulletin, 99 (2018) 349-358.

[135] Y. Zhang, J. Zhou, Q. Feng, X. Chen, Z. Hu, Chemosphere, 212 (2018) 523.

[136] C. Chang, X. Wang, Y. Bai, H. Liu, TrAC Trends in Analytical Chemistry, 39 (2012) 195-206.

[137] X. Zhao, S. Liu, Z. Tang, H. Niu, Y. Cai, W. Meng, F. Wu, J.P. Giesy, Scientific reports, 5 (2015) 11849.

[138] Z. Shi, C. Xu, H. Guan, L. Li, L. Fan, Y. Wang, L. Liu, Q. Meng, R. Zhang,

Colloids and Surfaces A: Physicochemical and Engineering Aspects, 539 (2018) 382-390.

[139] Q. Yang, S. Ren, Q. Zhao, R. Lu, C. Hang, Z. Chen, H. Zheng, Chemical Engineering Journal, 333 (2018) 49-57.

[140] Y. Chen, Z. Xiong, L. Peng, Y. Gan, Y. Zhao, J. Shen, J. Qian, L. Zhang, W. Zhang, ACS applied materials & interfaces, 7 (2015) 16338-16347.

[141] Y. Shao, L. Zhou, C. Bao, J. Ma, M. Liu, F. Wang, Chemical Engineering Journal, 283 (2016) 1127-1136.

[142] T. Wang, P. Zhao, N. Lu, H. Chen, C. Zhang, X. Hou, Chemical Engineering Journal, 295 (2016) 403-413.

[143] Z. Jiang, Y. Li, Journal of the Taiwan Institute of Chemical Engineers, 59 (2016) 373-379.

[144] L. Huang, M. He, B. Chen, B. Hu, Chemosphere, 199 (2018) 435-444.

[145] Y. Xu, J. Jin, X. Li, Y. Han, H. Meng, T. Wang, X. Zhang, Rsc Advances, 5 (2015) 19199-19202.

[146] L. Liu, J. Ge, L.T. Yang, X. Jiang, L.C. Qiu, Journal of Porous Materials, 23 (2016) 1-10.

[147] J. Fan, D. Chen, N. Li, Q. Xu, H. Li, J. He, J. Lu, Chemosphere, 191 (2018) 315.

[148] Z.Y. Zhang, Q.P. Lin, D. Kurunthu, T. Wu, F. Zuo, S.T. Zheng, C.J. Bardeen, X.H. Bu, P.Y. Feng, Journal of the American Chemical Society, 133 (2011) 6934-6937.

[149] X.L. Wang, X. Rong, H.Y. Lin, D.N. Liu, X. Wang, G.C. Liu, G. Song, Polyhedron, 126 (2017)

[150] X. Liu, W. Gong, J. Luo, C. Zou, Y. Yang, S. Yang, Applied Surface Science, 362 (2016) 517-524.

[151] X. Liu, J. Luo, X. Chen, Y. Yang, S. Yang, Chemical Research in Chinese Universities, 33 (2017) 268-273.

[152] A.X. Yan, S. Yao, Y.G. Li, Z.M. Zhang, Y. Lu, W.L. Chen, E.B. Wang,

Chemistry, 20 (2014) 6927-6933

[153] M. Huo, W. Yang, H.L. Zhang, L. Zhang, J.Z. Liao, L. Lin, C.Z. Lu, Rsc Advances, 6 (2016).

[154] S. Zhang, X. Wang, H.-X. Zhang, Z.-H. Zhao, X.-L. Wang, Chinese Chemical Letters, 29 (2018) 309-312.

[155] Z. Xie, W. Xu, X. Cui, Y. Wang, ChemSusChem, 10 (2017) 1645-1663.

[156] W. Teng, N. Bai, Z. Chen, J. Shi, J. Fan, W.-x. Zhang, Chemical Engineering Journal, 346 (2018) 388-396.

[157] B.N. Bhadra, S.H. Jhung, Microporous and Mesoporous Materials, 270 (2018) 102-108.

[158] J.Y. Song, B.N. Bhadra, N.A. Khan, S.H. Jhung, Microporous and Mesoporous Materials, 260 (2018) 1-8.

[159] A. Almasoudi, R. Mokaya, J. Mater. Chem., 22 (2012) 146-152.

[160] R.R. Salunkhe, Y.V. Kaneti, J. Kim, J.H. Kim, Y. Yamauchi, Acc Chem Res, 49 (2016) 2796-2806.

[161] S. Li, X. Zhang, Y. Huang, Journal of hazardous materials, 321 (2017) 711-719.

[162] Z. Abbasi, E. Shamsaei, S.K. Leong, B. Ladewig, X. Zhang, H. Wang, Microporous and Mesoporous Materials, 236 (2016) 28-37.

[163] H.Y. Lin, J. Zhao, G. Sheng, J. Luan, X.X. Liu, G.C. Liu, Dalton transactions, 46 (2017) 17067-17078.

[164] P. Pachfule, D. Shinde, M. Majumder, Q. Xu, Nature chemistry, 8 (2016) 718-724.

[165] S. Xu, Y. Lv, X. Zeng, D. Cao, Chemical Engineering Journal, 323 (2017) 502-511.

[166] X. Ma, L. Li, R. Chen, C. Wang, H. Li, H. Li, Chemistry, an Asian journal, (2018).

[167] Z. Song, W. Liu, N. Cheng, M. Norouzi Banis, X. Li, Q. Sun, B. Xiao, Y. Liu, A. Lushington, R. Li, L. Liu, X. Sun, Materials Horizons, 4 (2017) 900-907.

[168] N.L. Torad, M. Hu, S. Ishihara, H. Sukegawa, A.A. Belik, M. Imura, K. Ariga, Y.

Sakka, Y. Yamauchi, Small, 10 (2014) 2096-2107.

[169] L. Jin, X. Zhao, X. Qian, M. Dong, Journal of colloid and interface science, 509 (2018) 245-253.

[170] J. Zhang, X. Yan, X. Hu, R. Feng, M. Zhou, Chemical Engineering Journal, 347 (2018).

[171] Y. Song, T. Qiang, M. Ye, Q. Ma, Z. Fang, Applied Surface Science, 359 (2015) 834-840.

[172] E. Abdelillah Ali Elhussein, S. Şahin, Ş.S. Bayazit, Journal of Molecular Liquids, 255 (2018) 10-17

[173] S. Ru, L. Xu, H. Xiao, X. Li, Materials Research Express, 3 (2016) 115006.

[174] Y. Gu, K. Cheng, Y.-n. Wu, Y. Wang, C. Morlay, F. Li, ACS Sustainable Chemistry & Engineering, 4 (2016) 6744-6753.